

NOT SO HEAVY METALS: BLACK HOLE TRANSPORTED OXYGEN TO THE CIRCUMGALACTIC MEDIUM

N. NICOLE SANCHEZ¹, JESS WERK¹, MICHAEL TREMMEL², ANDREW PONTZEN³, CHARLOTTE CHRISTENSEN⁴, TOM QUINN¹,
 AKAXIA CRUZ¹, AND [Order subject to change]

¹Astronomy Department, University of Washington, Seattle, WA 98195, US, sanchenn@uw.edu

²Yale Center for Astronomy & Astrophysics, Physics Department, P.O. Box 208120, New Haven, CT 06520, USA

³Department of Physics & Astronomy, University College London, 132 Hampstead Road, London, NW1 2PS, United Kingdom and

⁴Physics Department, Grinnell College, 1116 Eighth Ave., Grinnell, IA 50112, United States

Submitted to The Astrophysical Journal

ABSTRACT

[UNDER CONSTRUCTION] We examine the effects of supermassive black hole (SMBH) feedback on the circumgalactic medium (CGM) using a cosmological hydrodynamic simulation (ROMULUS 25 Tremmel et al. 2017) and a set of zoom-in “genetically modified” Milky Way-mass galaxies sampling different evolutionary paths. We compare the column densities of OVI in Milky Way-mass galaxies and compare them with observations from the COS-Halos Survey; contrary to previous simulations which underpredicted the CGM column densities of OVI, these simulations are consistent with COS-Halos observations. We determine that a galaxy’s star formation history and accretion rate have little effect on the appearance of OVI in its CGM while column densities of OVI are more closely tied to galaxy halo mass. The set of zoom-in, genetically modified Milky Way-mass galaxies further confirm this result and demonstrate the effect of AGN feedback on the CGM’s OVI. We find that the SMBH acts as the physical mechanism for transporting metals out into its host halo thereby significantly impacting the appearance of OVI found in the CGM.

Subject headings: Gas physics – Galaxies: circumgalactic medium – Galaxies: spiral – Galaxies: kinematics and dynamics – Methods: Numerical

1. INTRODUCTION

The circumgalactic medium (CGM), the extended region of gas surrounding galaxies out to their virial radii, is a rich and vast yet mostly unexplored area of astronomy. Due to its diffuse nature, the CGM has remained one of the most difficult regions to observe. However, due to technological advances like the Cosmic Origins Spectrograph (COS) on the HST, researchers have finally begun observing this mysterious component of all galaxies. Observers have found it to be a structurally complex, multiphase medium ((Tumlinson et al. 2011; Werk et al. 2012, 2013, 2016; Tumlinson et al. 2017). Examinations like Werk et al. (2014) show that most of the “missing baryons” of galaxies likely reside in this diffuse region, implying that the CGM may play a key role in the growth of galaxies and the build up of their disks. Therefore, it is clear that understanding the CGM is crucial for understanding the complex nature of galaxy evolution and growth.

Several studies have been done to examine the effect of galaxy evolution on the CGM. The COS-Halo observations show a correlation between the column densities of OVI out to 150 kpc and the specific SFR of their observed galaxies. Higher abundances of OVI are found around SF galaxies compared to their passive counter parts. Openheimer 2016 argue that this bimodality arises due to the OVI acting as a proxy for the virial temperature of gas in these galaxy halos. Therefore, the more massive galaxies in the COS-Halo sample show less OVI in their CGM due to the intrinsically higher virial temperature of these massive red ellipticals. In contrast, Suresh et al. (2017) argue that the OVI is built up by AGN feedback, which can physically modify the CGM via outflows or heat it to the appropriate temperature for ionizing OVI.

In both cases, each argument implies an intrinsic link between the CGM and its host galaxy’s evolution.

Galaxy evolution has been shown to be strongly tied to the evolution of its central supermassive black hole (SMBH). Through relations like the M- σ and the bulge mass-BH mass correlation (Ferrarese & Merritt 2000; McConnell & Ma 2013), recent studies indicate that the SMBH and its host galaxy halo *co-evolve* (Gebhardt et al. 2000a; Ferrarese & Merritt 2000; McConnell & Ma 2013; Kormendy & Ho 2013, Reines 2015 and references therein). It is therefore unsurprising that the AGN is thought to leave its marks on the CGM. However, the direct mechanisms by which the AGN readily impacts the CGM are still hotly debated.

AGN may effect the CGM in a variety of ways. First, feedback from the active SMBH may inject energy into the surrounding material, raising temperatures, and ionizing metals in the gas [CITE]. Additionally, massive outflows of gas from the AGN may physically push gas out of the galaxy (some of which may end up falling back into the galaxy as part of the “recycling” of the CGM (Tumlinson et al. 2017, MORE), enriching CGM gas with metals from the center of the galaxy, and further enriching the IGM as gas is expelled from the galaxy halo. Cosmological hydrodynamic simulations have become a powerful tool for examining the physics driving the multiphase nature of the CGM [CITE].

Simulators have long been examining the underlying physics of AGN activity in galaxies; however, examining these effects in the diffuse region of the CGM is still a fairly new field ripe for discovery. Toward this end, we utilize a cutting-edge set of simulations: the cosmological volume, ROMULUS25 (Tremmel et al. 2017) and three “genetically modified” variations of

an isolated, zoom-in Milky-Way (MW) mass galaxy (Roth et al. 2016; Pontzen et al. 2017) simulated with and without the implementation of advanced BH physics (Tremmel et al. 2015). With these simulations, we plan to examine two specific questions with our study.

- How do the star formation and accretion history of the galaxy co-evolve with the CGM?
- How does AGN activity imprint itself on the CGM?

Both the ROMULUS25 simulation and our set of high-resolution, zoom-in simulations with genetic modifications will allow us to investigate the first question in detail. First, we examine the CGM in a range of MW-mass galaxies with varied morphologies from ROMULUS25. Additionally, from our isolated MW-mass galaxy and its subsequent “genetic modifications”, we quantify the effect of AGN feedback on the CGM by examining a set of galaxies run both with and without BH physics. Using these isolated, zoom-in simulations in tandem with the Romulus25 simulation, we illuminate the roles that stellar evolution and AGN feedback play in setting the properties of the CGM of MW-mass galaxies.

2. SIMULATION PARAMETERS

2.1. ChaNGa Physics

Both ROMULUS25 (hereafter R25) and our set of zoom-in galaxies were run using the smoothed particle hydrodynamics (SPH) N-body tree code, Charm N-body GrAvity solver [ChaNGa] (Menon et al. 2015). ChaNGa includes the same models for a cosmic UV background, star formation, ‘blastwave’ SN feedback, and low temperature metal line cooling as previously used in GASOLINE (Wadsley et al. 2004, 2008; Stinson et al. 2006; Shen et al. 2010). ChaNGa includes an improved SPH formalism which includes a geometric density approach in the force expression: $(P_i + P_j)/(\rho_i \rho_j)$ instead of $P_i/\rho_i^2 + P_j/\rho_j^2$ where P_i and ρ_i are the particle’s pressure and density, respectively. This update to the hydrodynamic treatment includes thermal diffusion (Shen et al. 2010) and reduces artificial surface tension allowing for better resolution of fluid instabilities (Ritchie & Thomas 2001; Menon et al. 2015; Governato et al. 2015). Additional improvements have been made to the BH formation, accretion, and feedback models as well as an improved prescription for dynamical friction (Tremmel et al. 2015, 2017).

Our simulations were run with a Λ CDM cosmology from the most recent Planck collaboration utilizing $\sigma_0 = 0.3086$, $\alpha = 0.6914$, $h = 0.67$, $\sigma_8 = 0.77$ and have Plummer equivalent force softening lengths of 250 pc. For simulating the cosmic reionization energy, both simulations enact a UV background at $z \sim 9$ (Haardt & Madau 2012).

2.2. Romulus 25 Cosmological Volume

The ROMULUS25 (Tremmel et al. 2017) simulation is a cosmological volume which includes galaxy halos within the mass range $10^8 - 10^{13} M_\odot$. R25 has a mass resolution of $3.4 \times 10^5 M_\odot$ and $2.1 \times 10^5 M_\odot$ for DM and gas particles, respectively. For our study, we focus on galaxies within the MW-mass halo regime, $5 \times 10^{11} M_\odot - 2 \times 10^{12} M_\odot$.

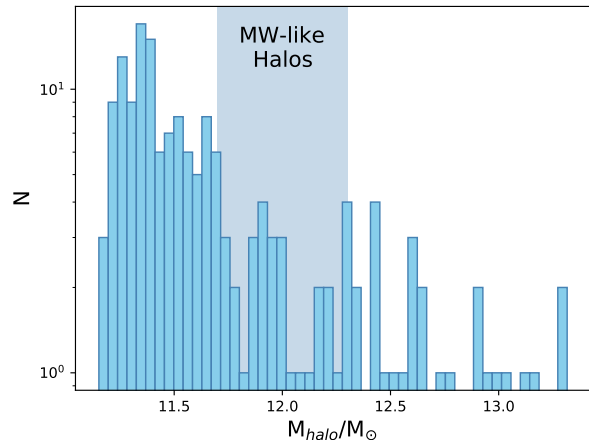


FIG. 1.— R25 is an SPH simulated cosmological volume with galaxy halos spanning the orders of $10^8 - 10^{13} M_\odot$. For clarity, we’ve plotted a histogram of only the galaxies in the volume with masses between $2 \times 10^{11} M_\odot - 2 \times 10^{13} M_\odot$ (The latter is the upper limit of galaxy masses in the volume.) The shaded region indicates the “MW” mass range, $5 \times 10^{11} M_\odot - 2 \times 10^{12} M_\odot$, from which we select our 25 galaxies.

$10^{12} M_\odot$ (Figure 1). We examine all the galaxies within the specified mass range and exclude any galaxies within twice the virial radius of another galaxy, thereby removing galaxies that might be satellites of a larger galaxy. With these selection criteria in place, our sample includes 25 galaxies.

2.3. Zoom-In Galaxies: Patient 0 and its Genetic Modifications

To select our galaxy, we ran initial uniform-volume, $50 h^{-1}$ Mpc on a side, dark matter-only cosmological volume. From this volume a MW-mass halo at $z=0$, was selected as our “Patient 0” and then re-simulated at a higher resolution. For the subsequent, “genetically modified” (GM) zoom-in runs, we utilize the same method of modification as Pontzen et al. (2017). These GM simulations keep the large scale structure and cosmological conditions Λ CDM consistent (as in Patient 0), while allowing for modifications of their accretion histories (Roth et al., 2015). Patient 0 (and its 3 GM simulations) have a mass resolutions of $1.4 \times 10^5 M_\odot$ and $2.1 \times 10^5 M_\odot$ for DM and gas particles, respectively. The DM field in these galaxies is simulated at twice the gas linear resolution to reduce noise in the potential near the galactic center (Pontzen et al. 2017) and more accurately trace black hole dynamics (Tremmel et al. 2015).

2.3.1. Galaxies with BH Physics

At $z = 0$, our “Patient 0” (hereafter P0) galaxy is a star forming galaxy with a disk (Figure 2a). P0 has an incoming satellite at $z = 1$ with an original mass of $7.34 \times 10^{10} M_\odot$ (mass ratio, $q = 0.12$). For each GM galaxy simulation, we systematically shrink this satellite halo’s mass prior to its merger with the main halo. (Table 1) GM1 results in a similar disk, star forming galaxy as P0, while GM2 and GM3 become quenched at $z \sim 1$ (Figure 2a).

While the GM galaxies utilize the same process as Pontzen et al. (2017), their study examines a different set

TABLE 1
ZOOM-IN GALAXIES PROPERTIES *with BHs* AT $z = 0.17$ Values that have been updated are *italicized*

Sim	Total Halo Mass (M_\odot)	Total Gas Mass (M_\odot)	Total Stellar Mass (M_\odot)	CGM Gas Mass (M_\odot)	R_{vir} (kpc)	T_{vir} (K)	Satellite Mass (M_\odot)
P0	1.08×10^{12}	1.09×10^{11}	5.71×10^{10}	<i>9.32×10^{10}</i>	268.9	5.12×10^5	7.34×10^{10}
GM1	1.07×10^{12}	1.01×10^{11}	6.43×10^{10}	<i>8.39×10^{10}</i>	269.2	5.12×10^5	5.86×10^{10}
GM2	8.69×10^{11}	7.41×10^{10}	1.38×10^{10}	<i>6.89×10^{10}</i>	254.1	$X \times 10^5$	3.97×10^{10}
GM3	7.76×10^{11}	6.36×10^{10}	1.04×10^{10}	<i>5.02×10^{10}</i>	241.7	4.14×10^5	2.45×10^{10}

TABLE 2
ZOOM-IN GALAXIES PROPERTIES *without BHs* AT $z = 0.17$

Sim	Total Halo Mass (M_\odot)	Total Gas Mass (M_\odot)	Total Stellar Mass (M_\odot)	CGM Gas Mass (M_\odot)	R_{vir} (kpc)	T_{vir} (K)	Satellite Mass (M_\odot)
P0noBH	8.36×10^{11}	7.0×10^{10}	7.37×10^{10}	$X \times 10^{10}$	262.8	$X \times 10^5$	7.34×10^{10}
GM1noBH	8.38×10^{11}	7.07×10^{10}	7.34×10^{10}	$X \times 10^{10}$	263.0	$X \times 10^5$	5.86×10^{10}
GM2noBH	8.42×10^{11}	7.08×10^{10}	7.33×10^{10}	$X \times 10^{10}$	263.4	$X \times 10^5$	3.97×10^{10}
GM3noBH	8.43×10^{11}	7.19×10^{10}	7.28×10^{10}	$X \times 10^{10}$	263.5	$X \times 10^5$	2.45×10^{10}

of galaxies. The three galaxies in Pontzen et al. (2017) were run to $z = 2$ and have $M_{Halo} \sim 10^{12}$. They each have incoming satellites whose masses are both increased and decreased prior to merging with the main galaxy, as in our galaxies; however, the resulting effect of their modifications were different from ours, as we explore in Section 4.

2.3.2. Galaxies without BH Physics

One key benefit of the individual zoom-in galaxies include the ability to remove or adjust the physical parameters affecting our galaxies to test different theoretical models which would be too computationally expensive to do with a large volume like R25. We utilize this benefit to further understand the effects of the AGN. To isolate the effect of the AGN on the CGM, all four of the zoom-in simulations (P0 and its 3 GMs) were re-simulated at the same resolution and with all the same physics *excluding* BH formation, feedback, and dynamical friction (Table 2). Black hole seed formation was disabled and the BH feedback and accretion efficiency parameters were set to 0.

2.3.3. Quenching in GM2 and GM3

Particularly of note, the top panel of Figure 2, which shows star formation histories of the four zoom-in galaxies with BH physics included, clearly shows that unlike P0 and GM1 which remain star forming throughout their history, GM2 and GM3 become quenched at $z \sim 1$. This immediate quenching just after the merger of the satellite with the main halo is particularly interesting because it does not take effect in the set of zoom-in galaxies without BH physics. Contrastingly, the lower panel of Figure 2 shows the star formation histories of the four zoom-in galaxies without BH physics and all four of their histories are nearly identical. The stark differences between the GM2 and GM3 galaxies with and without BHs imply that some interplay between the satellite's mass and the AGN feedback must play a pivotal role in quenching these galaxies so thoroughly.

We further examine the effects of the BH by looking to the mass buildup and accretion rate of the BHs. The

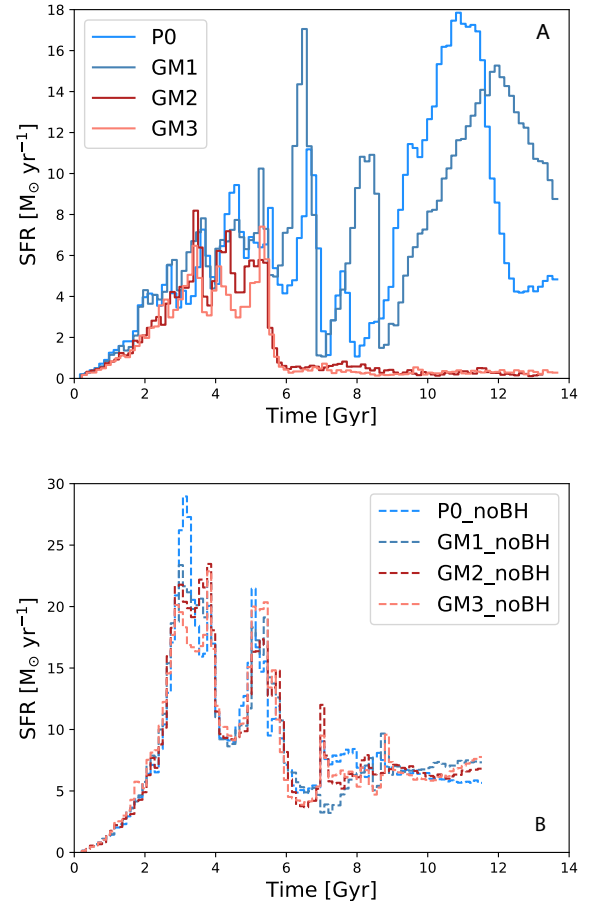


FIG. 2.— The star formation histories for the zoom-in galaxies: Patient 0 and its 3 GM galaxies with BH physics (*Upper*) and *Lower* without BH physics. In the galaxies including BH physics, P0 and GM1 remain star forming throughout their histories while GM2 and GM3 become quenched at $z \sim 1$. Without BH physics, all four galaxies remain star forming until $z = 0$. This is an effect we will explore in future work.

upper panel in Figure 3 shows the SMBH mass as a func-

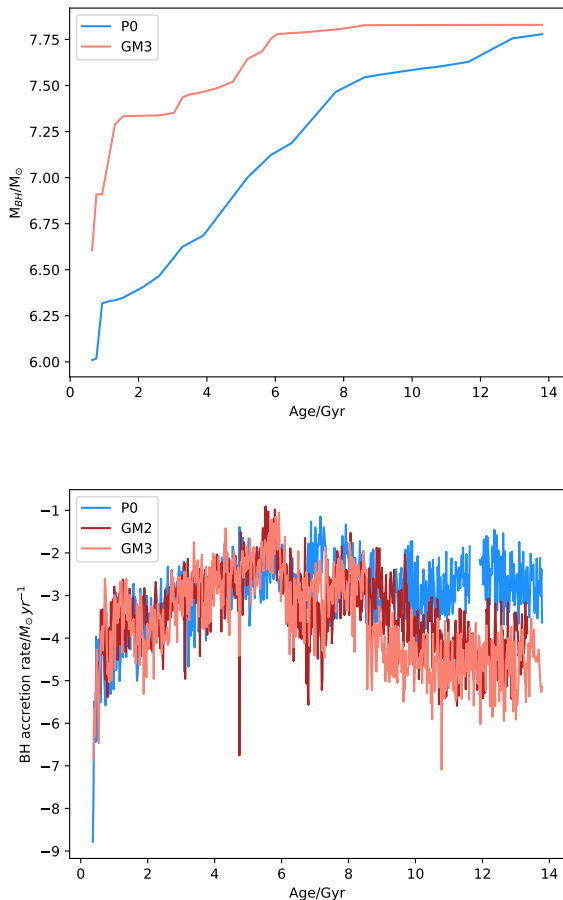


FIG. 3.— SMBH mass (*Upper*) and SMBH accretion rates (*Lower*) for our 4 zoom-in galaxies. Colors as in Figure 7. The SMBH growth of GM2 and GM3 occurs quicker than the growth of the SMBH in the two star forming zoom-in galaxies. In particular, GM3, which has the most significant modification to its satellite’s mass, has a SMBH that grows quickest. Both quenched galaxies also have a sharp peak in accretion rate around the time of the merger with the satellite ($z \sim 1$, $t \sim 6$ Gyr), indicated by the dashed grey line.

tion of time. Here we see that the mass growth in the quenched galaxies, GM2 and GM3, occurs earlier in comparison to the star forming galaxies, especially in the case of GM3. A similar result can also be seen in lower panel of Figure 3 which depicts the SMBH accretion rate as a function of time. It is clear from this figure that an increase of accretion occurs near the time of the merger, $z \sim 1$ or $t \sim 6$ Gyr. It is clear from the BH’s activity and growth that the effect of the mass of the incoming satellite has profound affect on the assembly history of this galaxy. Pontzen et al. (2017) previously explored the relationship between BH feedback and mergers and its effect on quenching, using the same genetic modification technique as we use for the GM galaxies in our study. They determine that AGN feedback is critical to quenching a galaxy, which is consistent with our finding that the only quenched galaxies are in simulations that include SMBHs. Pontzen et al. (2017) argues that the merger can disrupt the cold disk of the galaxy, which then allows the feedback of the AGN to have a farther reaching effect on the star forming gas of the disk thereby keeping

the galaxy in a state of quiescence. We note however, that the genetic modifications performed on the galaxies of (Pontzen et al. 2017) was different from the ones implemented here. In their case, it was an increase of the satellite’s mass that resulted in a quenched galaxy, rather than a shrinking as we affect here.

This set of galaxies, which were produced from very similar initial conditions but which illustrate very different star formation and accretion histories, allows us to directly examine how assembly history may imprint itself on the CGM. However, the specific effects of the AGN’s accretion on the assembly history of the galaxy is beyond the scope of this paper. We leave an examination of the quenching mechanisms of these galaxies to future work.

3. RESULTS

3.1. Qualitative CGM Properties

Individual halos in the ROMULUS25 cosmological volume and in the individual zoom-in galaxies are extracted using the Amiga Halo Finder (AHF) (Knollmann & Knebe 2009) and central SMBH positions and velocities are defined relative to the center position and inner 1 kpc center-of-mass velocity of their host halo, respectively. From R25, we specifically examine Milky Way-mass halos which are defined as halos between 5×10^{11} and $2 \times 10^{12} M_\odot$ and are at least twice a virial radii from their nearest neighbor (to exclude any satellites). All zoom-in galaxies are isolated with a minor merger at $z \sim 1$.

The CGM of each individual galaxy halo (within the R25 galaxies and our zoom-ins) is defined as the mass enclosed in an annulus from 10 kpc from the center position out to a virial radius defined as the radius at which 200 times the critical density, ρ_c , where $\rho/\rho_c = 200$. Figure 4 shows the phase diagrams of the CGMs of the 4 zoom-in galaxies with and without BH physics. Examining the CGM phase diagrams for the GMs that include BH physics (*Left Column*), we note the following key differences: less overall mass from the uppermost (P0) to lowermost (GM3) figure; variations in the amount of cool, dense gas ($T < 10^{4.5}$, $n_H > 10^{-3}$); and the lack of hot, dense gas ($T > 10^{5.5}$, $n_H > 10^{-3}$) in the phase diagrams of GM2 and GM3, our quenched galaxies. Similarly, examining the CGM phase diagrams that *exclude* BH physics (*Right Column*), we don’t see any significant differences.

The first of the differences between CGM phase diagrams with BH physics is unsurprising, as it correlates directly with the final halo mass of the galaxies. P0 results in the most massive halo at $z \sim 0$, while GM3 results in the least massive (Table 1). The second of these differences [FINISH ANALYSIS ON COOL DENSE TAIL].

We are most interested in the last difference: the lack of the hot, dense gas in the quenched galaxies that is present in the star forming galaxies, P0 and GM1. We note that this feature is also present in the CGM diagrams of the galaxies *without* BH physics, which all result in star forming, disked galaxies. Figure 5 further examines this difference with the same CGM phase diagrams of P0 and GM2 colored by mass, metallicity, and distance from the center of the galaxy, with (*Two Upper Rows*) and without (*Two Lower Rows*) BH physics. The hot, dense gas in P0 with BH physics (*Upper Row*) appears to

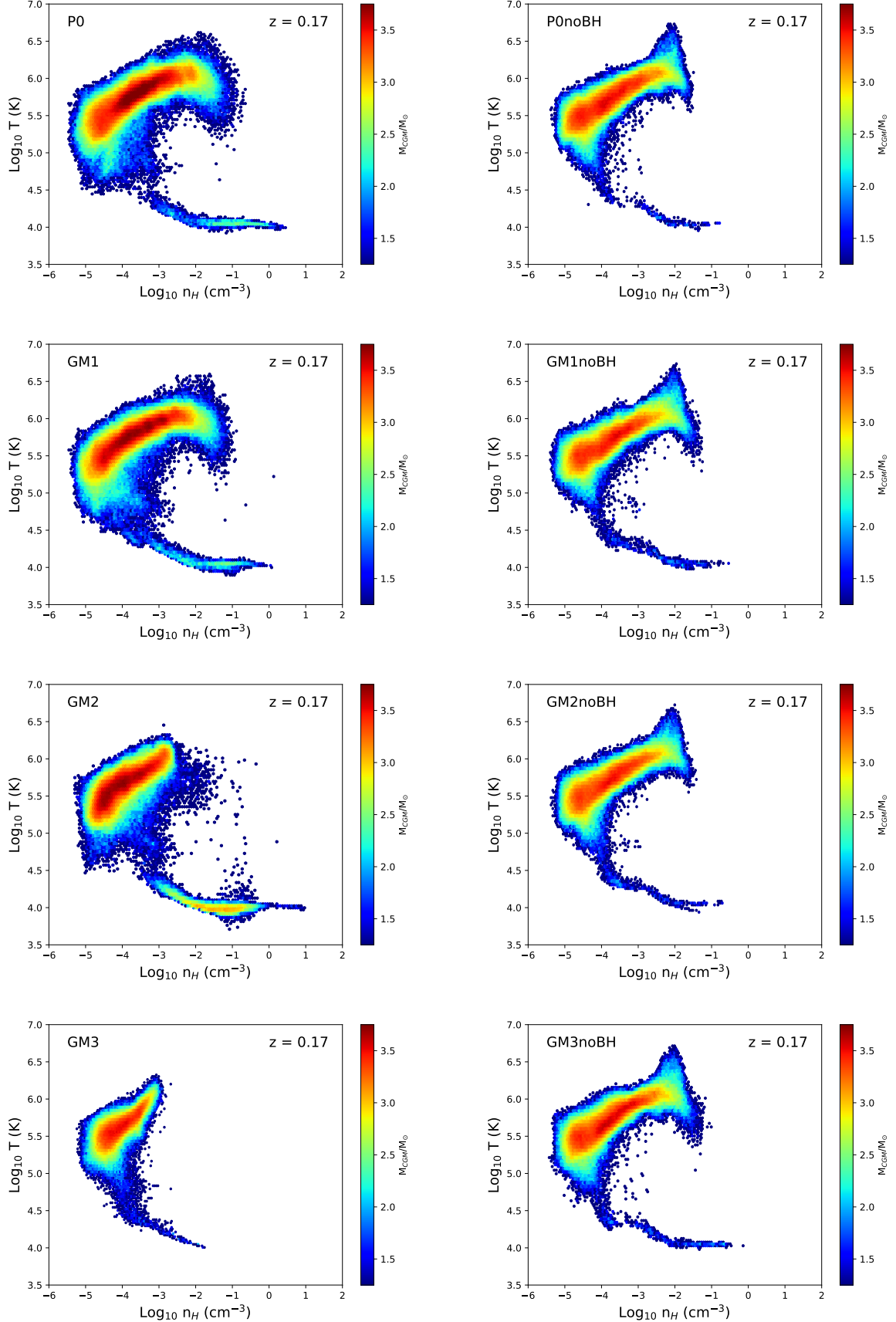


FIG. 4.— Phase diagrams of the temperature and density of the two star forming zoom-in galaxies, P0 (*Top row*) and GM1 (*Second row*), and the two quenched galaxies, GM2 (*Third row*) and GM3 (*Bottom row*). The phase diagrams of galaxies with BH hole physics vary quite widely between the star forming (P0 and GM1) and quenched cases (GM2 and GM3), particularly in the highest temperature and density gas. However, the phase diagrams of the galaxies without BH physics appear nearly identical, as do their star formation histories (Figure 2 lower panel).

be mostly comprised of high metallicity gas that is close to the disk ($R < 50$ kpc). Further examining this gas, we find that 3 % of the CGM gas has metallicity $Z > Z_{\odot}$ at $z = 0.17$. Furthermore, of this 3 %, 23 % is between 10 and 20 kpc from the center of the galaxies. For GM1, the CGM is comprised of 7.6 % gas with $Z > Z_{\odot}$ with nearly 50 % of that gas between 10 and 20 kpc. Contrastingly, a negligible amount of the CGM of both GM2 and GM3 have $Z > Z_{\odot}$ at $z = 0.17$. The CGMs of the four galaxies without BH physics also have small amounts of gas with $Z > Z_{\odot}$, from 0.1 % in P0noBH to 0.04 % in GM3noBH. These percentages of high metallicity gases in P0 and GM1 with BH physics point to metal exchange in the galaxy that is strongly dependent on the SMBH (which we discuss further in Section 3.3). It's interesting to note that the removal of the BH physics in all four zoom-ins makes little difference in the final gas phase properties of the main halo (Table 2). Nevertheless, the differences we see in the CGMs of these galaxies, both with and without BH physics, don't seem to have a significant effect on the OVI that we see in the galaxies, as we explore below.

3.2. OVI as a Tracer for Virial Temperature

Column densities of OVI are calculated using the analysis software Pynbody (Pontzen 2013). Oxygen abundances is traced throughout the integration of the simulation and ionization states are calculated during post-processing, assuming optically thin conditions and a Haardt & Madau (2012) ultraviolet radiation field at $z = 0$. Recent papers [CITE] have raised concerns that this UV background is too strong [CITE]; however, since our primary concern is the abundance of OVI which is considered to be collisionally ionized rather than photoionized [CITE], our choice of UV background should not affect our results. We use the CLOUDY software package (Ferland et al. 1998; Stinson et al. 2012) to create models with varying temperature, density, and redshift to determine OVI fractions for all the gas in each simulated galaxy. Figure 6 shows the column densities of OVI as a function of radius (**Need to change this to impact parameter; Current profiles are created when galaxies are in a face-on orientation.**) for our 25 R25 MW-mass galaxies. Red and blue lines describe quenched and star forming galaxies within the sample, respectively. The COS-Halo Survey dataset is plotted on top in black, with squares and circles distinguishing between elliptical and spiral galaxies. Upper and lower limits are designated with arrows and unfilled markers. The R25 galaxies well match the observations from the COS-Halo Survey; however, we note that they are systematically higher than the upper limits of the more massive ellipticals in the survey. (See 4) We further compare the column densities of OVI in the R25 galaxies to the 4 zoom-in galaxies with BH physics and find that these galaxies also well match the observed column densities of COS-Halo and fall within the range of the R25 galaxies (Figure 6b).

Figures 6 and 7 make it clear that our simulations reproduce the column densities of OVI in the CGM; however, this conclusion is not the only important feature of these plots. In addition, we note that *the column densities of OVI in the CGMs of these galaxies does not seem to depend on the assembly history of the galaxy*. We see this in both R25, which in addition to providing evidence

for this initial result also gives cosmological credence to our suite of GM galaxies, and our four GM galaxies that include BH physics. We confirm our result with Patient 0 and its GMs, which include two star forming galaxies and two quenched galaxies, all of which well match the observations of COS-Halo despite differing formation histories. (Figure 7)

Figure 8 shows the average fractions for all the ions of oxygen within three mass ranges: low mass ($5 \times 10^{10} - 5 \times 10^{11} M_{\odot}$), Milky Way-mass ($5 \times 10^{11} - 2 \times 10^{12} M_{\odot}$), and high mass ($2 \times 10^{12} - 2 \times 10^{13} M_{\odot}$). The OVI fractions decrease from the MW-mass range to the high mass regime due to the increase in virial temperature which moves from a value close to the ionization peak for OVI, $\sim 10^{5.5} K$ to $10^{6.3} K$. From this study, we determine that morphological evolution of the galaxy doesn't correlate with the evolution of the CGM, as described by the column densities of OVI. Instead, it appears that the mass of the galaxy, and connectedly its virial temperature [Table 1], plays a more significant role in determining the amount of OVI seen in the CGM.

3.3. Metal Transport by the SMBH

We examine the column densities of OVI in the CGMs of our 4 zoom-in galaxies *without* BH physics and compare them to the cases where BH physics is included. Figure 7 shows the column densities of OVI in the CGM of all four of our zoom-in galaxies with BH physics (solid lines) and without (dashed lines). We can see that in the cases where BH physics is not included, the values of N_{OVI} are significantly lower implying that the presence of the AGN must play an important role in populating OVI in the CGM. We look to the temperature, mass, density, and metallicity of the CGM to investigate the cause of this decrease in OVI. (Figure 9)

The difference between the CGMs of these two cases appears to come directly from the change in metallicity due to the lack of black hole activity. (Figure 9) We examine the metallicity of the disk to look for further clues about how the lack of AGN activity is affecting the galaxy. Figure 10 shows that, in the galaxies without BH physics, the metals produced in the disk aren't driven into the CGM due to the lack of AGN feedback. This result is also consistent with what we see in Figure 5. The lack of high metallicity ($Z > Z_{\odot}$) in the CGM phase diagrams of the galaxies with no BH physics (*Right Column*) confirms the fact that metals are not being driven out of the disk. Surprisingly, however, the feedback doesn't seem to play a role in significantly heating or excavating the CGM gas, but it appears the the AGN's feedback is pivotal in *transporting the metals* from the center of the galaxy out into the CGM. *The AGN plays a significant role in physically driving the metals out of the disk and into the outer regions of the CGM.*

[Include discussion about metal flux into and out of galaxy (once complete); comparisons between observations and amount of total metals in disk (plus metal gradients)]

4. DISCUSSION

Questions to expound on: Limitations of the simulations Comparisons with other groups: Oppenheimer, Suresh, Hummels(Fire)? What questions remain/are raised by results

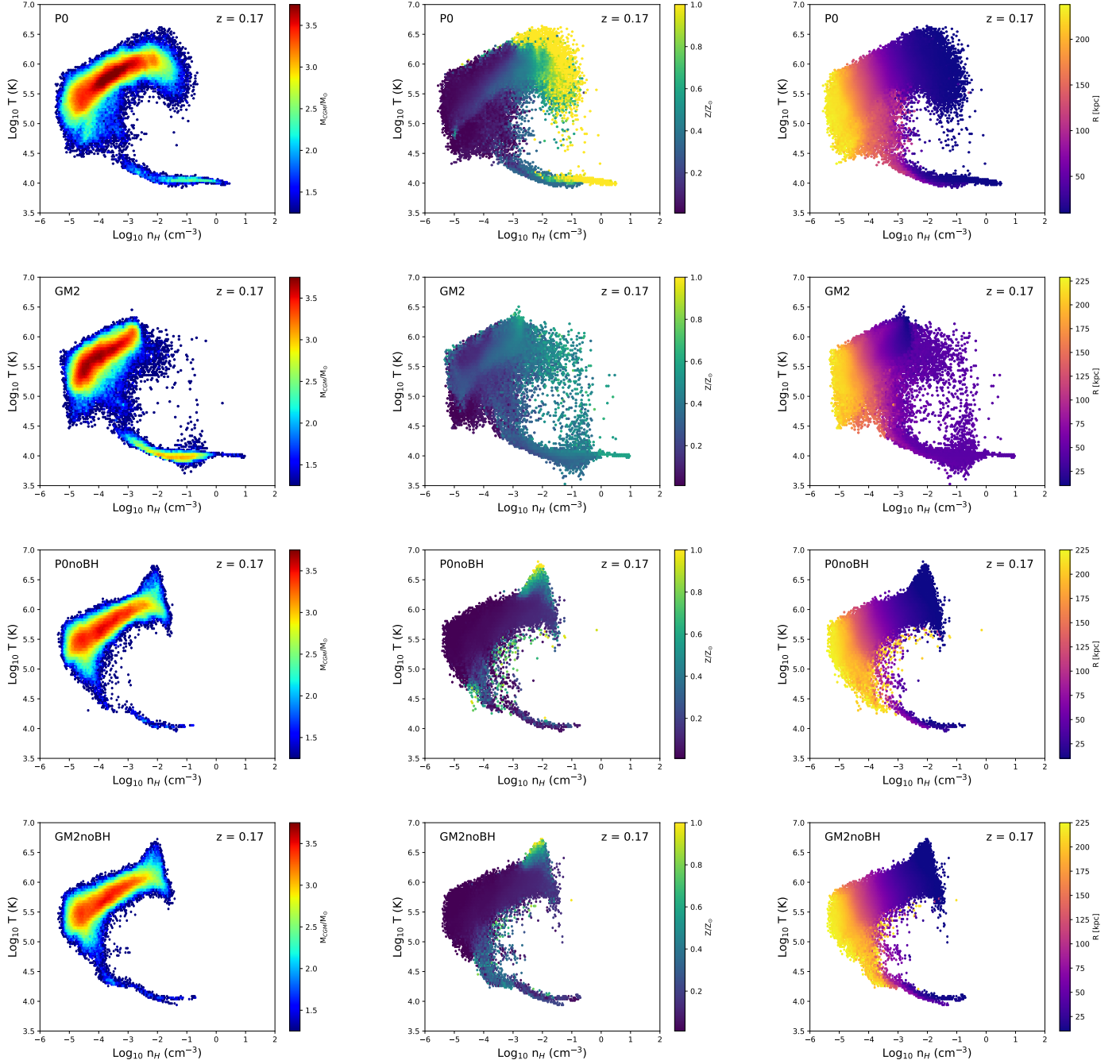


FIG. 5.— Phase diagrams of the temperature and density of the star forming zoom-in galaxy, P0 (*Top row* with BH physics, *Middle row* without), and the quenched galaxy, GM2 (*Bottom row*). *Left:* As we noted, the phase diagrams of galaxies with BH hole physics show stark differences between the star forming (P0 and GM1) and quenched cases (GM2 and GM3). particularly in the highest temperature and density gas. *Middle:* The same phase diagram showing temperature and density, however, the colorbar is weighted by the average metallicity of the star in each bin. We note that the high density, high temperature gas we see in the star forming P0, is also the highest metallicity gas in the CGM. *Right:* Similarly, a phase diagram with the colorbar now weighted by the average distance from the center of the galaxy of the gas particles in each bin. The concentration of gas at high density and temperature *and* high metallicity also appears to be the gas closest to the center of the galaxy. However, this gas is also not present in the noBH physics case. We conclude that due to the active star formation in P0 in tandem with the AGN physics at play, this excess of gas comes from gas that has been ejected from the disk due to AGN feedback. Therefore explaining it's significant absence from the phase diagrams of P0 without BH physics and GM2.

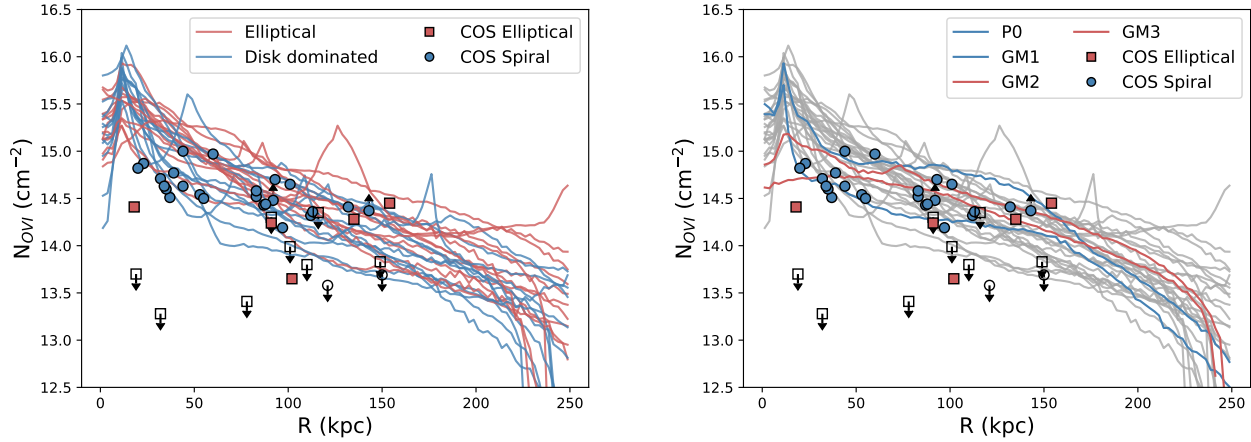


FIG. 6.— *Left*: Mean column densities of OVI as a function of radius for all Milky Way mass halos in the R25 simulation. Blue and red lines distinguish between disk dominated spirals and quenched elliptical galaxies within the R25 simulation. *Right*: Column densities of OVI in our 4 zoom-in galaxies. Grey lines indicate R25 MW galaxy column densities from *Left*. Blue solid lines describe our two star forming galaxies, P0 and GM1. GM4-7, our passive galaxies, are in solid red. Filled circles and squares indicate spirals and ellipticals from the COS-Halo Survey dataset. Unfilled squares indicate upper limits.

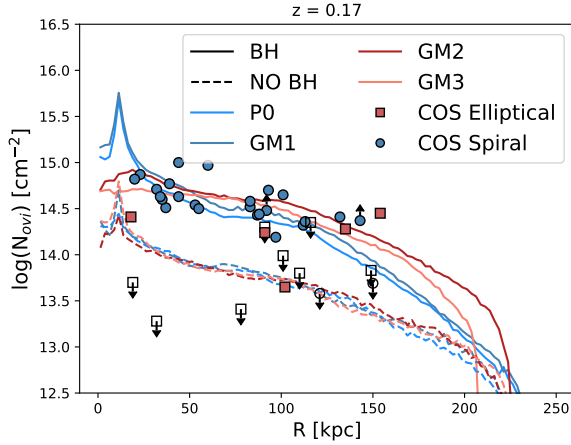


FIG. 7.— Column density profiles of OVI in our 4 zoom-in galaxies with (solid lines) and without (dashed lines) BH physics. P0 and GM1, our two star forming galaxies are colored as light blue and dark blue, respectively. Our quenched galaxies, GM2 and GM3, are labeled in dark red and pink, respectively.

5. CONCLUSION

Result 1: OVI as a Tracer for Virial Temperature of the Halo

The combined, consistent results of the cosmological R25 and our 4 zoom-in galaxies (which include BH physics) imply a mechanism by which column densities of OVI are set by the virial temperature of the CGMs host galaxy. They aren't affected by the evolution of a disk. Their phase diagrams also lack significant difference in their overall assembly history, except where more gas is clearly present in the higher mass galaxies. Therefore, we surmise that the differences in the CGM are not determined by whether or not a galaxy quenches but rather these conditions for OVI are primarily set by the virial temperature of the galaxy.

These results are consistent with those of Oppenheimer et. al. 2016 who used a suite of EAGLE simulated galaxies to examine the bimodality of OVI column densities (further discussed in [Tumlinson 2011]) in star forming

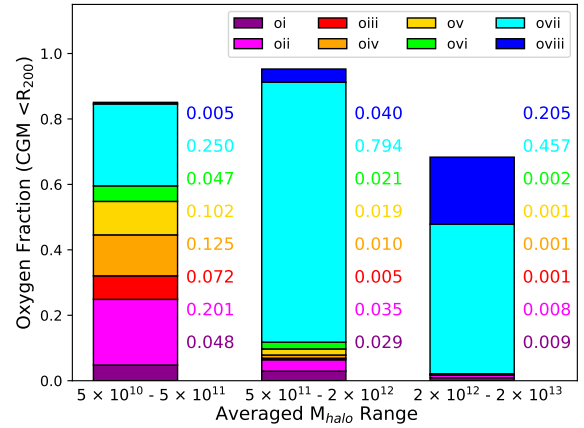


FIG. 8.— Oxygen ion fractions in the CGM of our 25 MW-mass galaxies and 11 high mass galaxies from R25. Log M_{halo} for each halo are labeled in white text. [Under construction]

and quenched galaxies. They argue that the star forming galaxies ($10^{11} - 10^{12}$), which were found to have a higher fraction of OVI, were at the right virial temperature to maximize OVI production, while their quenched galaxies ($10^{12} - 10^{13}$) had high enough virial temperatures such that the dominant ionization state was not OVI but rather OVII or above. Oppenheimer et. al. 2016 argues that the OVI content was not a tracer of star formation directly, but rather a more direct thermometer for the temperature of the halo.

We note that the quenched galaxies in our sample are smaller in mass than our star forming galaxies, unlike those in Oppenheimer, explaining the lack of bimodality that we observe. While all the GMs are in the mass range to have virial temperatures which optimize OVI, we further examine the R25 simulation's higher mass, passive galaxies in addition to the MW-mass galaxies (which have virial temperatures spanning 5.8×10^5 K $\mid 1.1 \times 10^6$ K) to see if the bimodality appears. (Figure 8) We determine that the OVI still provides a direct thermometer for the temperature of the halo. [Under

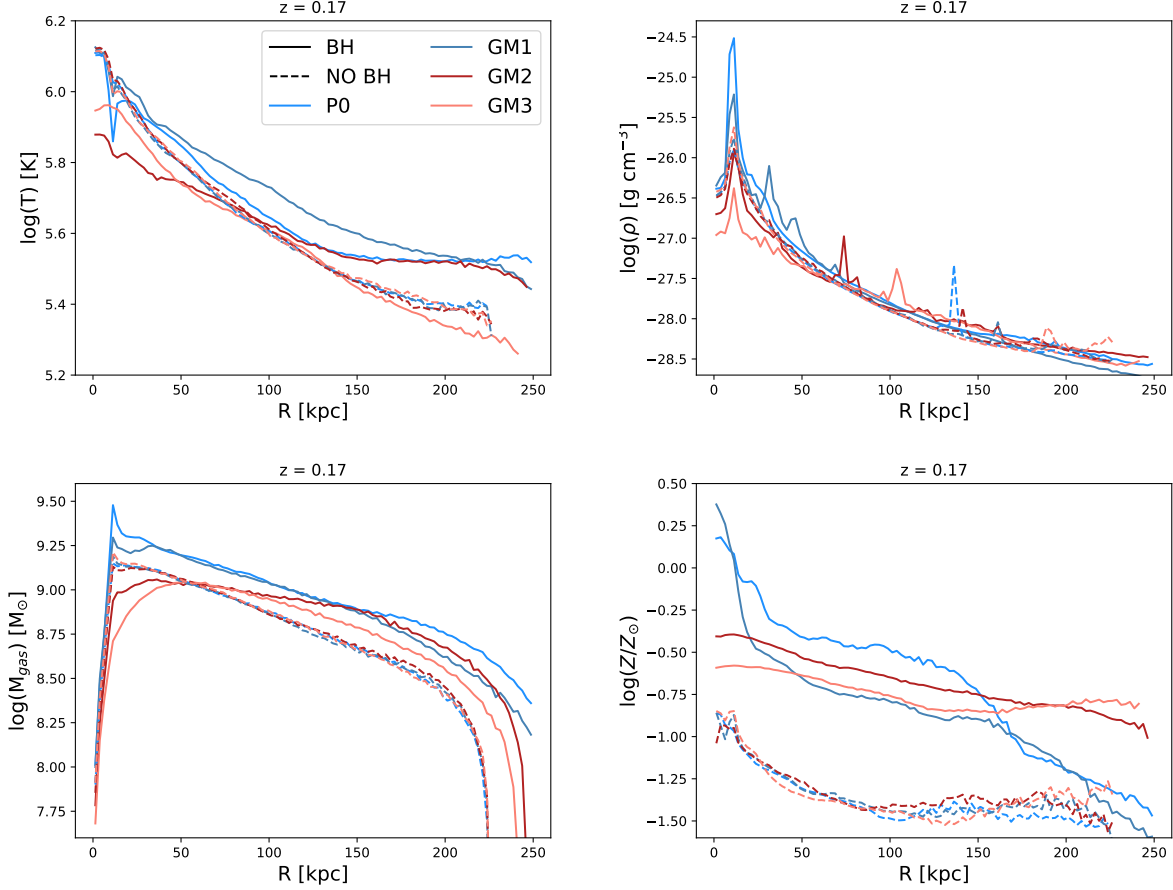


FIG. 9.— Temperature, Total Mass, Total Density, and Metallicity profiles of the CGM of our 4 zoom-in galaxies with and without BH physics. Colors and linestyles as in Figure 7.

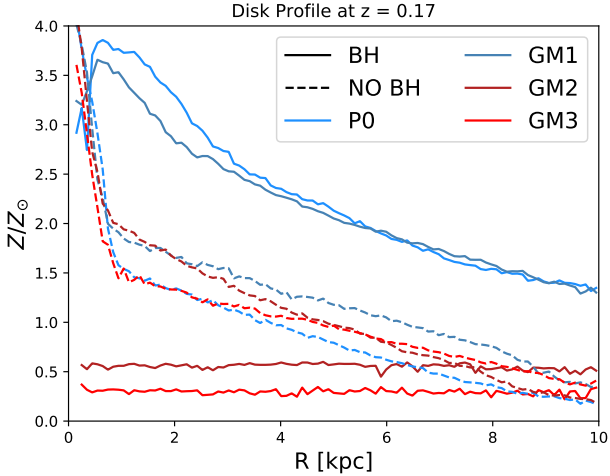


FIG. 10.— Metallicity profile of the gas within the disk of our 4 zoom-in galaxies with and without BH physics. Colors and line styles as in Figure 9. Without the black hole physics, metals remain trapped near the center of the disk with no mechanism to propagate out into the CGM.

construction]

Furthermore, examining galaxies with masses larger than our MW-mass GMs ($> 2 \times 10^{12}$) from the R25 suite,

we see that the column densities of OVI decrease as the ionization peak of OVI is surpassed by these halos. Since the virial temperature is higher, the oxygen is likely to be ionized to a higher ionizations state (OVII or OVII), which we show is the case in Figure 8. [Under construction]

Result 2: AGN as driver for metals in the CGM

Our result that the AGN acts a physical driver for metals in the CGM has interesting consequences. Previous studies have examined the effect of heating on the CGM as the AGNs energy input may put the gas into phases which optimize the production of OVI. (Suresh et al. 2017) Others have proposed that the feedback from AGN may physically drive outflows of gas out of the galaxy, resulting in a lower density CGM and therefore lower densities of OVI. Neither of these cases are what we see. *Instead, we see a suite of CGM which rely on the AGN for the propagation of metal mass (but not total gas mass) into the outer galaxy and OVI columns which depend on the virial temperature of the galaxy.* (Figure 10)

Acknowledgements

REFERENCES

- Ferland, G., Korista, K., Verner, D., et al. 1998, Publications of the Astronomical Society of the Pacific, 110, 761 3.2
- Ferrarese, L., & Merritt, D. 2000, The Astrophysical Journal, 539, L9 1

- Governato, F., Weisz, D., Pontzen, A., et al. 2015, *Monthly Notices of the Royal Astronomical Society*, 448, 792 [2.1](#)
- Haardt, F., & Madau, P. 2012, *The Astrophysical Journal*, 746, 125 [2.1](#), [3.2](#)
- Knollmann, S. R., & Knebe, A. 2009, *The Astrophysical Journal Supplement Series*, 182, 608 [3.1](#)
- McConnell, N. J., & Ma, C.-P. 2013, *The Astrophysical Journal*, 764, 184 [1](#)
- Menon, H., Wesolowski, L., Zheng, G., et al. 2015, *Computational Astrophysics and Cosmology*, 2, 1 [2.1](#)
- Pontzen, A., Tremmel, M., Roth, N., et al. 2017, *Monthly Notices of the Royal Astronomical Society*, 465, 547 [1](#), [2.3](#), [2.3.1](#), [2.3.3](#)
- Ritchie, B. W., & Thomas, P. A. 2001, *Monthly Notices of the Royal Astronomical Society*, 323, 743 [2.1](#)
- Roth, N., Pontzen, A., & Peiris, H. V. 2016, *Monthly Notices of the Royal Astronomical Society*, 455, 974 [1](#)
- Shen, S., Wadsley, J., & Stinson, G. 2010, *Monthly Notices of the Royal Astronomical Society*, 407, 1581 [2.1](#)
- Stinson, G., Seth, A., Katz, N., et al. 2006, *Monthly Notices of the Royal Astronomical Society*, 373, 1074 [2.1](#)
- Stinson, G. S., Brook, C., Prochaska, J. X., et al. 2012, *Monthly Notices of the Royal Astronomical Society*, 425, 1270 [3.2](#)
- Suresh, J., Rubin, K. H. R., Kannan, R., et al. 2017, *Monthly Notices of the Royal Astronomical Society*, 465, 2966 [1](#), [5](#)
- Tremmel, M., Governato, F., Volonteri, M., & Quinn, T. R. 2015, *Monthly Notices of the Royal Astronomical Society*, 451, 1868 [1](#), [2.1](#), [2.3](#)
- Tremmel, M., Karcher, M., Governato, F., et al. 2017, *Monthly Notices of the Royal Astronomical Society*, 470, 1121 ([document](#)), [1](#), [2.1](#), [2.2](#)
- Tumlinson, J., Peebles, M. S., & Werk, J. K. 2017, *Annual Review of Astronomy and Astrophysics*, 55, 389 [1](#)
- Tumlinson, J., Thom, C., Werk, J. K., et al. 2011, *Science*, 334, 948 [1](#)
- Wadsley, J., Stadel, J., & Quinn, T. 2004, *New Astronomy*, 9, 137 [2.1](#)
- Wadsley, J. W., Veeravalli, G., & Couchman, H. M. P. 2008, *Monthly Notices of the Royal Astronomical Society*, 387, 427 [2.1](#)
- Werk, J. K., Prochaska, J. X., Thom, C., et al. 2012, *The Astrophysical Journal Supplement Series*, 198, 3 [1](#)
- . 2013, *The Astrophysical Journal Supplement Series*, 204, 17 [1](#)
- Werk, J. K., Prochaska, J. X., Tumlinson, J., et al. 2014, *The Astrophysical Journal*, 792, 8 [1](#)
- Werk, J. K., Prochaska, J. X., Cantalupo, S., et al. 2016, 24 [1](#)